NASA TN D-1437

TECHNICAL NOTE

D-1437

OPTICAL TORQUEMETER FOR HIGH ROTATIONAL SPEEDS

By Alois Krsek, Jr., and Marvin Tiefermann

Lewis Research Center
Cleveland, Ohio

NATIONAL AERONAUTICS AND SPACE ADMINISTRATION

WASHINGTON

October 1962

NATIONAL AERONAUTICS AND SPACE ADMINISTRATION

TECHNICAL NOTE D-1437

OPTICAL TORQUEMETER FOR HIGH ROTATIONAL SPEEDS

By Alois Krsek, Jr., and Marvin Tiefermann

SUMMARY

A remote-reading torquemeter that was developed for cryogenic-pump and turbine research is described. By use of optical methods, it is possible to avoid physical contact with the rotating shaft and, also, to permit limited radial and axial movement of the shaft. An accuracy of 1 percent of full load at 50,000 rpm is possible. The instrument can be calibrated statically. Tests were made to evaluate temperature and high-speed effects. Dynamic comparisons were made with a cradled electric dynamometer.

INTRODUCTION

The purpose of this report is to describe a torquemeter developed at the Lewis Research Center. Present rocket-pump and turbine research and development require a remote-reading torquemeter usable to 50,000 rpm that can be calibrated statically and has an accuracy of 1 percent of full load. Typical requirements for full-load torque for various applications range from 100 to 26,400 inch-pounds. The system must be independent of ±1/8-inch axial and/or radial displacements of the torque shaft.

A literature survey revealed that no commercial torquemeter was available that could meet these requirements. At low speeds, strain-gage torquemeters (ref. 1) and other types with sliprings work satisfactorily. Above 20,000 rpm, noise and rapid wear of the brushes make sliprings undesirable. Magnetic types are sensitive to axial or radial displacements of the torque shaft. Electric dynamometers, which absorb power, are also unsuitable for some phases of turbine-pump research.

An angular-twist torquemeter with an optical electromechanical measuring system was developed and evaluated at the Lewis Research Center. The measuring system has no physical contact with the rotating shaft. A static calibration of the torquemeter was performed, and the effect of temperature on the torquemeter was investigated. The zero-torque output was checked at various speeds up to 50,000 rpm. Because

of limited facilities, no dynamic calibrations were made. However, dynamic comparison tests were made over a limited speed and torque range with an electric dynamometer.

The optical system is discussed in the appendix by Donald R. Buchele.

APPARATUS AND PROCEDURE

Torquemeter

The torquemeter consists essentially of three main parts: a shaft, an optical system, and a readout servosystem.

The shaft (fig. 1) consists of a torsional spring section between two rigid sections. On each rigid section is a flat, polished, light-reflecting surface, which measures 1 by $1\frac{1}{2}$ inches and rotates as an integral part of the shaft. The reflectors are approximately in the same plane and parallel to the axis of rotation. The surfaces are ground and lapped to a 4-microinch finish and polished to give an efficient light-reflecting surface. The surfaces are also flat to within four helium light bands. A length of $7\frac{1}{2}$ inches between reflectors was chosen so that the spring section could be designed to give a 2° to 3° deflection for full load. This full-load torsional stress was approximately equal to one-half the elastic limit. The diameter of either a hollow or a solid shaft was also determined by other design considerations such as couplings, means of shaft support, and critical rotational speeds. The design of the rigid sections was determined by the type of coupling used, such as flanges with dowel pins, splines, or keyways. The rigid sections were made symmetrical to facilitate dynamic balancing.

The shafts discussed were made of either SAE 4340, heat-treated Rc 28-32, or stainless 17-4 PH condition - H 900.

The optical system, shown schematically in figure 2, consists of a lamp masked with a narrow slit, the long dimension of which is in the plane of the figure. Light passing through this slit is collimated by lens L_1 and reflected from the first rotating reflector A to a fixed reflector R_1. The light beam is converged by lens L_2 and reflected off fixed reflectors R_2, R_3, and R_4 to lens L_3. The light is recollimated by lens L_3 and reflected from the second rotating reflector B to the final image lens L_4. This lens forms an image of the light-source slit at Q.

The principle of optical-motion compensation and the specific functions and spacing of the individual optics are described in the appendix.

The final image of the light-source slit is stationary and does not rotate or sweep because of rotation of the shaft. The final image is intermittent because of the limited time the light is incident on rotating reflectors A and B.

When torque is applied to the shaft, reflector B may be considered as being rotated at an angle relative to reflector A, and the final image of the slit is displaced. The displacement is proportional to the rotation of B with respect to A.

A photograph of the optical system is shown in figure 3. All the lenses are achromatic and have approximate diameters of 2 inches. The compensating lenses each consist of two closely mounted lenses with an effective focal length of 4.4 inches. The collimating lens is similar, but it has an effective focal length of 3.8 inches. The image lens is an achromatic lens with a 10-inch focal length. All fixed reflectors are first-surface mirrors 1/4-inch thick, $2\frac{3}{8}$-inches high, and approximately $1\frac{1}{4}$-inches wide. The light-source slit is 1/8 by 1/32 inch and is illuminated by an air-cooled projection lamp with an internal reflector. All components are mounted on a 3/4-inch stress-relieved steel base.

The readout servosystem (figs. 4 and 5) consists of two selenium photovoltaic cells, $1\frac{11}{16}$ by $\frac{7}{8}$ inch, that can integrate the light pulses. The cells are mechanically coupled to a two-phase balancing motor and a three-turn wire-wound precision output potentiometer. Electrically, the cells in series opposition are connected to a servoamplifier that drives the balancing motor and positions the cells so that the gap or space between the two cells follows the final image. The output voltage from the bridge formed by the zero potentiometer and the output potentiometer is a linear function of the cell displacement. Full-scale response time of the servosystem is approximately 2 seconds.

The relation between the torque and the output voltage is shown in the following manner: The output voltage of the servosystem (fig. 4) is

$$e = Cd \tag{1}$$

where C is a constant dependent upon the input voltage E and the mechanical coupling between the photocells and the output potentiometer, and d is the displacement of the output image. This displacement is

$$d = f \tan 2\theta$$

where f is the focal length of the image lens and θ is the twist angle of the shaft due to an applied torque. When θ is small,

$$d \cong 2f\theta \tag{2}$$

The relation between θ and torque is

$$\theta = \frac{T}{K} \tag{3}$$

where T is the applied torque and K is the torsional spring constant. Substitution of equations (2) and (3) into (1) gives

$$e = \frac{2fc}{K} T \tag{4}$$

The output voltage is a linear function of torque.

From the derivation of the output voltage, the displacement of the output image $d \cong 2f\theta$. The displacement is 1 inch for a 3° angle of twist and an image lens with a 10-inch focal length. For 1 percent accuracy, then, the photocells had to be repositioned to 0.01 inch.

Test Procedure

The effect of shaft displacement relative to the optical system was investigated by moving the optical and readout servosystems with respect to the rotating shaft. The displacements were $\pm 1/8$ inch in the axial and radial directions.

Static calibrations were performed with the apparatus shown in figure 6. One end of the shaft was fixed to a rigid plate. The other end was fastened to a 60.00-inch moment arm and supported by a ball-bearing pedestal. The moment arm was designed and counterweighted so that its center of gravity coincided with the axis of rotation in order to eliminate the effects of moment-arm mass. The end of the moment arm was machined to a 60.00-inch radius to maintain a constant moment-arm length as the shaft was twisted. Connected to the end of the arm was the wire on which the calibrated weights were hung. The ball-bearing

pedestal was designed to load the shaft in torsion only and to minimize bending and shear stresses.

Field calibration of the readout servosystem is accomplished with a zero-span bar. A photograph of the zero-span bar with the torquemeter assembly is shown in figure 7. One side of the bar has two reflectors in the same plane; the other side has two reflectors at a fixed angle of approximately 2°. The parallel reflectors simulate the unstressed torque shaft, and the other side of the bar represents the shaft stressed to approximately two-thirds of full load. The two flat surfaces at the center of the zero-span bar were used as support areas during the polishing of the end surfaces. After a calibration curve for a shaft is established, the zero-span bar is substituted for the shaft, and a point is found on the calibration curve that is equivalent to the fixed angle. This point then can be used to set the span of the readout servosystem in the field.

The effects of temperature on the readout servosystem were checked by temperature cycling the optical and servosystem (minus the amplifier) in an insulated box in which the temperature was controlled from 30° to 120° F. Stationary reflectors R_6 and R_7, cemented to their mounts, caused large temperature errors because of bending similar to that of a bimetallic strip. A mount that permitted the reflector and the mount to move independently eliminated most of this error. The final correction was accomplished by adding a temperature-sensitive nickel-wire resistor (R_T in figs. 4 and 5) to the output bridge of the servosystem.

A test for zero shift and sensitivity of the torquemeter was made with zero applied torque. A 4-inch-tip-diameter air turbine was used to drive an unloaded shaft to 50,000 rpm for the zero-applied-torque tests. A solid 1-inch-diameter shaft was used to avoid any torsional vibrations because the free end of the shaft had little or no damping. At various speeds the servosystem was unbalanced manually, and the output of the photocells was measured. The readout servosystem was then allowed to rebalance from both directions to check for any dead zone in the system.

Dynamic comparisons were made with the optical torquemeter and an electric absorption dynamometer. The dynamometer was rated at 300 horsepower at 5000 rpm and was cradled by self-alining trunnion bearings between two pedestals. The dynamometer reaction was measured with a commercial self-balancing torque cell. A gear box with a 2.2 gear ratio was coupled to the dynamometer. The gear box was cradled by hydrostatic bearings between two pedestals. The optical torquemeter was coupled between the high-speed shaft of the gear box and an 11.56-inch-mean-diameter air turbine, which produced the driving force. The speed and torque ranges were varied and controlled by changing the field current

in the electric dynamometer. Before the comparison tests, the dynamometer was calibrated. The comparison tests were run at speeds of 4100, 5270, 5860, and 6450 rpm over a torque range of 600 to 1260 inch-pounds. The full-load torque for the shaft used in the optical torquemeter during these tests was 2160 inch-pounds.

RESULTS AND DISCUSSION

Relative shaft displacement with respect to the optical system of ±1/8 inch in the axial or the radial direction had no effect on the output.

Figure 8 gives a summary of the static calibrations of four shafts; the deviation from linearity is plotted against applied torque. The maximum deviation is ±0.4 percent of full load, but most of the points are within ±0.2 percent of full load. Full-load torque of the shafts tested ranges from 100 to 26,400 inch-pounds. Change in span is accomplished by designing each shaft to twist approximately 3° for full-load torque. The optical system and the readout servosystem are then standard for all ranges.

Typical zero shift due to the temperature change of the torquemeter is shown in figure 9. This shift would be the error contributed by the optical system and the readout servosystem if the torquemeter zero adjustment was made at one temperature and a reading was taken at another temperature. The two curves are for readings with and without compensation. Maximum deviation after compensation was ±0.2 percent of full load for a ±50° F change in temperature.

Reference 1 shows the temperature effects on the torsional modulus. The angle of twist is inversely proportional to the torsional modulus. For a ±50° F change in the temperature from 80° F, the angle of twist will change approximately ±0.5 percent; that is, the torque reading will be in error by ±0.5 percent.

In the zero-shift zero-applied-torque test, the cell output was constant from 3000 to 50,000 rpm. Below 3000 rpm, the combination of the photovoltaic cells and the input circuit would not integrate the light pulses. Since all the applications for the torquemeter were above 3000 rpm, no attempt was made to correct the input circuit.

The readout servosystem did not have any hysteresis, but the output did shift about 0.2 percent of full load at 50,000 rpm. The only loading on the shaft was caused by windage and bearing friction, which accounted for only a small portion of the torque indicated.

The results of the dynamic comparison of the torquemeter and the dynamometer are presented in figure 10. The difference between the two is given in percent of full load of the torquemeter plotted against torque. Maximum deviation is ±1 percent, and most of the points are within ±0.5 percent. No systematic error could be found from the data.

SUMMARY OF RESULTS

An optical torquemeter for high rotational speeds was developed and evaluated, and the following results were obtained:

1. Small shaft displacements (radial or axial ±1/8 in.) due to floating bearings or thermal expansions did not affect the accuracy of torque indication.

2. The torquemeter could be calibrated statically.

3. Temperature effects on the readout servosystem and the optical system were within ±0.2 percent of full load for a ±50° F change in temperature; the temperature effect on the shaft could be calculated.

4. At 50,000 rpm, the photovoltaic cells were capable of detecting the light pulses, and the torquemeter had no zero shift.

5. The dynamic comparison of the torquemeter with the cradled electric dynamometer showed agreement to within 1 percent.

6. The maximum torque range (26,400 in.-lb) of the shafts used in this investigation was not maximum for this device. Full-scale torque would depend only on the ability to design a shaft with the proper torsional spring constant.

7. The summation of errors from the individual tests performed showed the optical torquemeter to have an accuracy of 1 percent of the full-load reading under the conditions of an actual cryogenic-pump or turbine test.

Lewis Research Center
National Aeronautics and Space Administration
Cleveland, Ohio, June 12, 1962

APPENDIX - THE OPTICAL SYSTEM

By Donald R. Buchele

Torque Indication

Neglect motion compensation and consider only a torque applied to the stationary shaft. Torque indication may be obtained when reflector A in figure 2 is fixed while the shaft at reflector B is twisted, because the collimated beam leaving B deflects twice the angle of twist. The collimated beam is focused at the final image, which deflects to give a torque indication.

It is desirable to obtain light transmission to the final image for as great an angle of shaft rotation as possible, so that adequate flux is available to the photovoltaic cell, and a limited amount of torque oscillation can be averaged. These considerations are aided by use of lenses L_2 and L_3 in the optical path. During 12° shaft rotation the full flux is transmitted, and beyond 20° it falls to zero. The averaging of torque oscillation can be extended by placing a number of reflectors around the shaft instead of at A and B only.

Motion Compensation

Motion is compensated when the direction of the collimated beam leaving reflector B is unchanged for shaft rotation and translation in three orthogonal axes. Although the collimated beam may be displaced by such shaft motion, the final image at Q is stationary because it is at the focus of the collimated beam. The image is displaced only by angular deflection of the collimated beam.

Shaft rotation about its axis is shown in figure 11(a). This is an elevation view of figure 2 with the optical path unfolded between reflectors A and B. The shaft rotation at A, therefore, appears in the opposite direction to that at B. Lens L_2 forms an intermediate image that sweeps vertically with shaft rotation. By symmetry of lenses L_2 and L_3, the beam leaving B is stationary as the shaft rotates.

Reflectors A and B at the periphery of the shaft of radius r move vertically at the same time they rotate. For maximum flux transmission, the lenses L_2 and L_3 are placed at a distance $f + r/2$ from the shaft axis, where f is the focal length. The beam leaving A thus follows the displacement of B, and it is cutoff symmetrically by interception at the rims of lenses L_2 and L_3.

Lenses L_2 and L_3 should have a flat field at the intermediate image to maintain collimation of the beam at B and a sharp focus at the final image. The achromatic lenses, when oriented for minimum spherical aberration and coma at the plane $r/2$ from the shaft axis, yield the desired flat field very closely.

The collimated beam at A and B in figure 2 is at a small angle from a normal to the shaft axis in order to avoid interference of the optical elements along the light path; therefore, the intermediate image describes a shallow arc instead of a straight vertical line as the shaft rotates. This motion could cause a small angular deviation in the plane of figure 2 of the beam leaving B. The motion is compensated when the beam leaving B is parallel to the beam incident upon A.

Shaft rotation about a vertical axis is shown in the plan view in figure 11(b), which corresponds to figure 2 without lenses and with two fixed reflectors. Rotation of the shaft through an angle $\alpha/2$ is compensated by an even number of reflections; so, the beam leaving B is not deviated. In the actual system shown in figure 2, five reflections by mirrors R_1, R_2, R_3, R_4, and R_5 plus an intermediate image formed by lenses L_2 and L_3 are equivalent to an even number of two reflections.

Shaft rotation about an axis in the plane of figure 2 and perpendicular to the shaft axis displaces reflectors A and B in their own plane; thus, no compensation is needed. Shaft translation in any direction does not change the direction of the beam leaving B, since it is collimated at both A and B, and they are flat surfaces.

REFERENCE

1. Rebeske, John J., Jr.: Investigation of a NACA High-Speed Strain-Gage Torquemeter. NACA TN 2003, 1950.

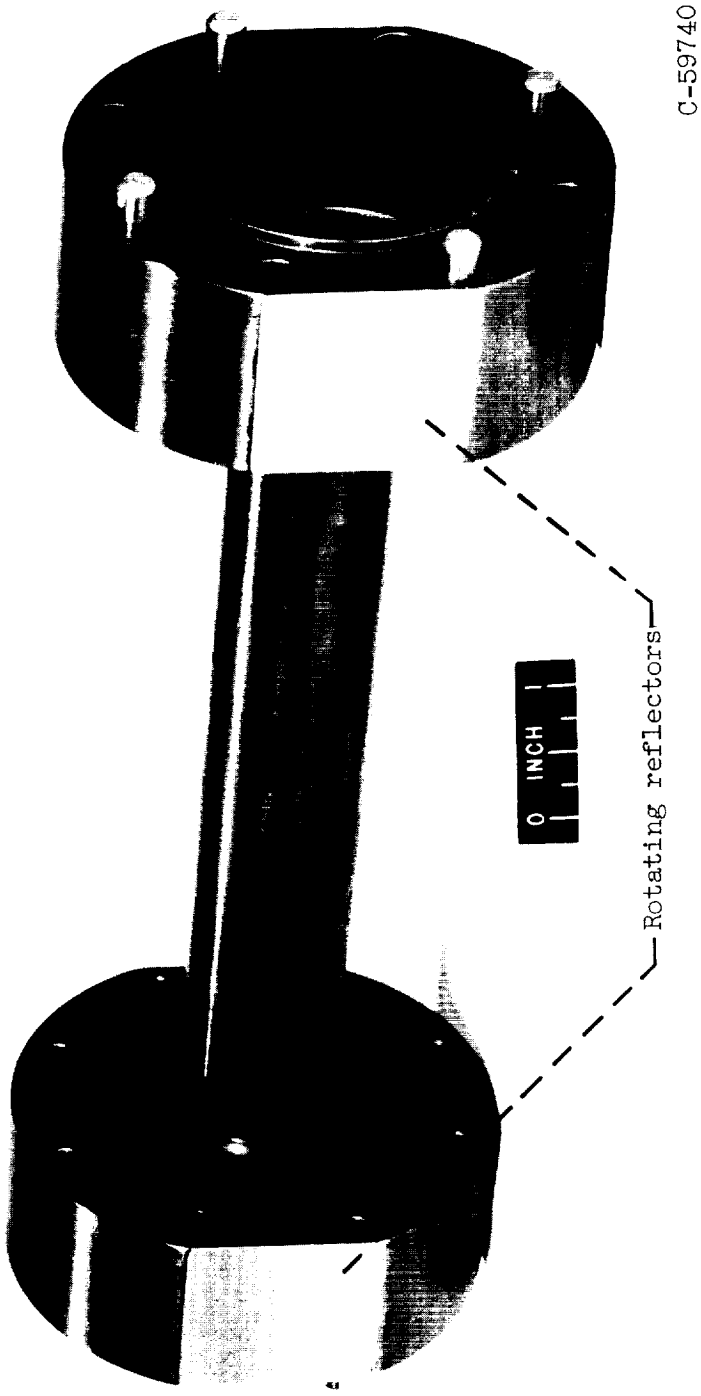

Figure 1. - Shaft.

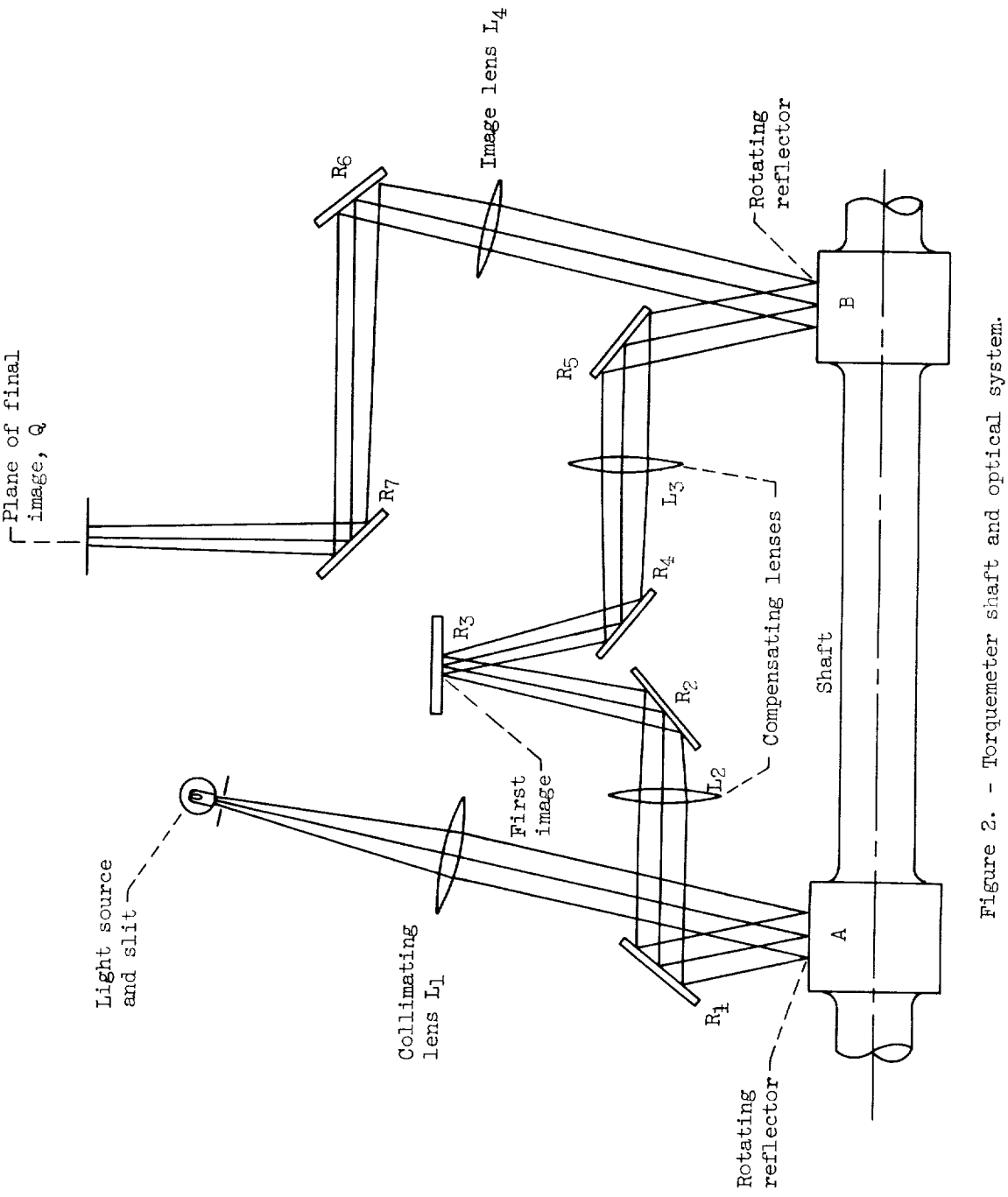

Figure 2. - Torquemeter shaft and optical system.

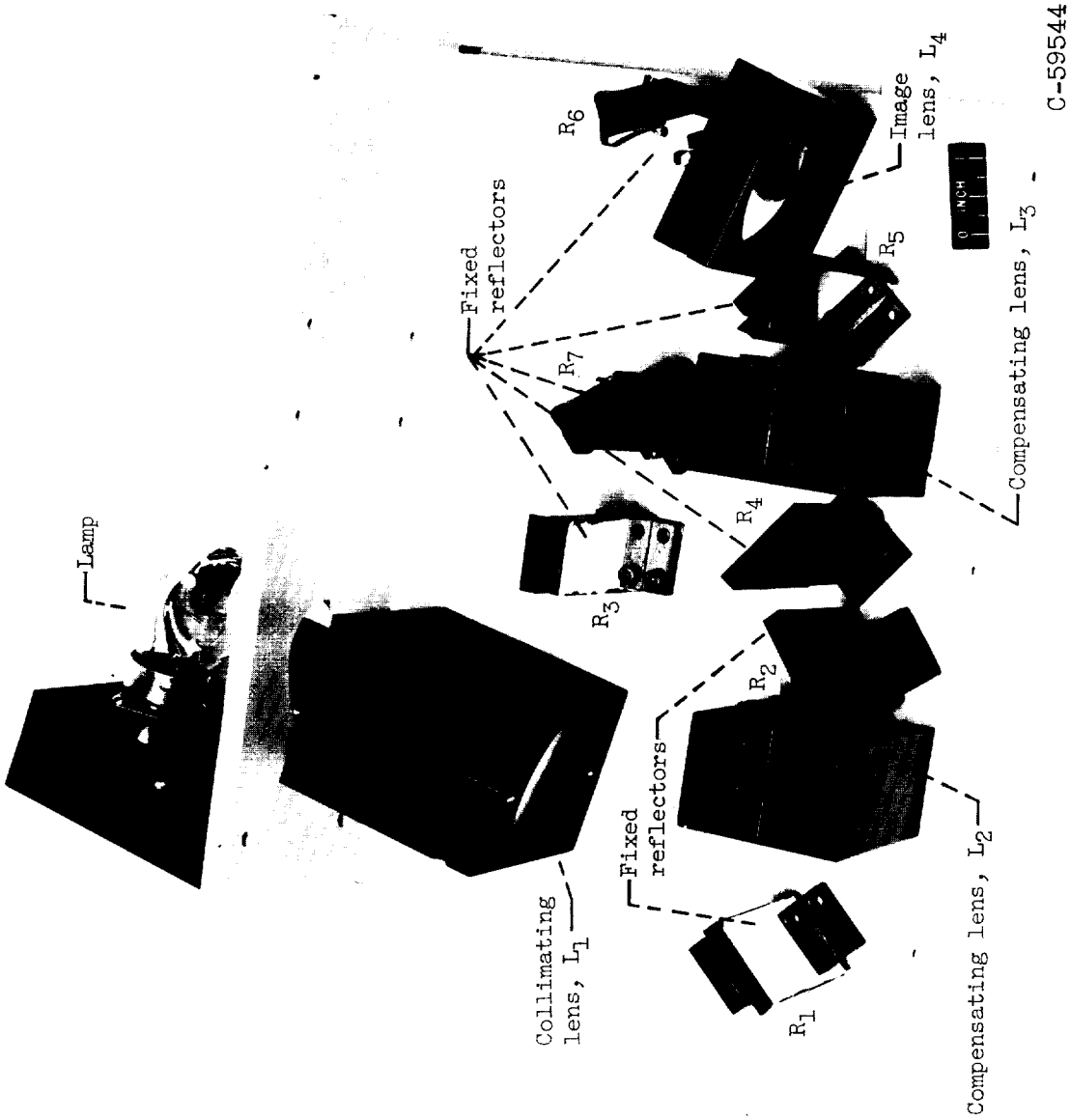

Figure 3. - Optical system.

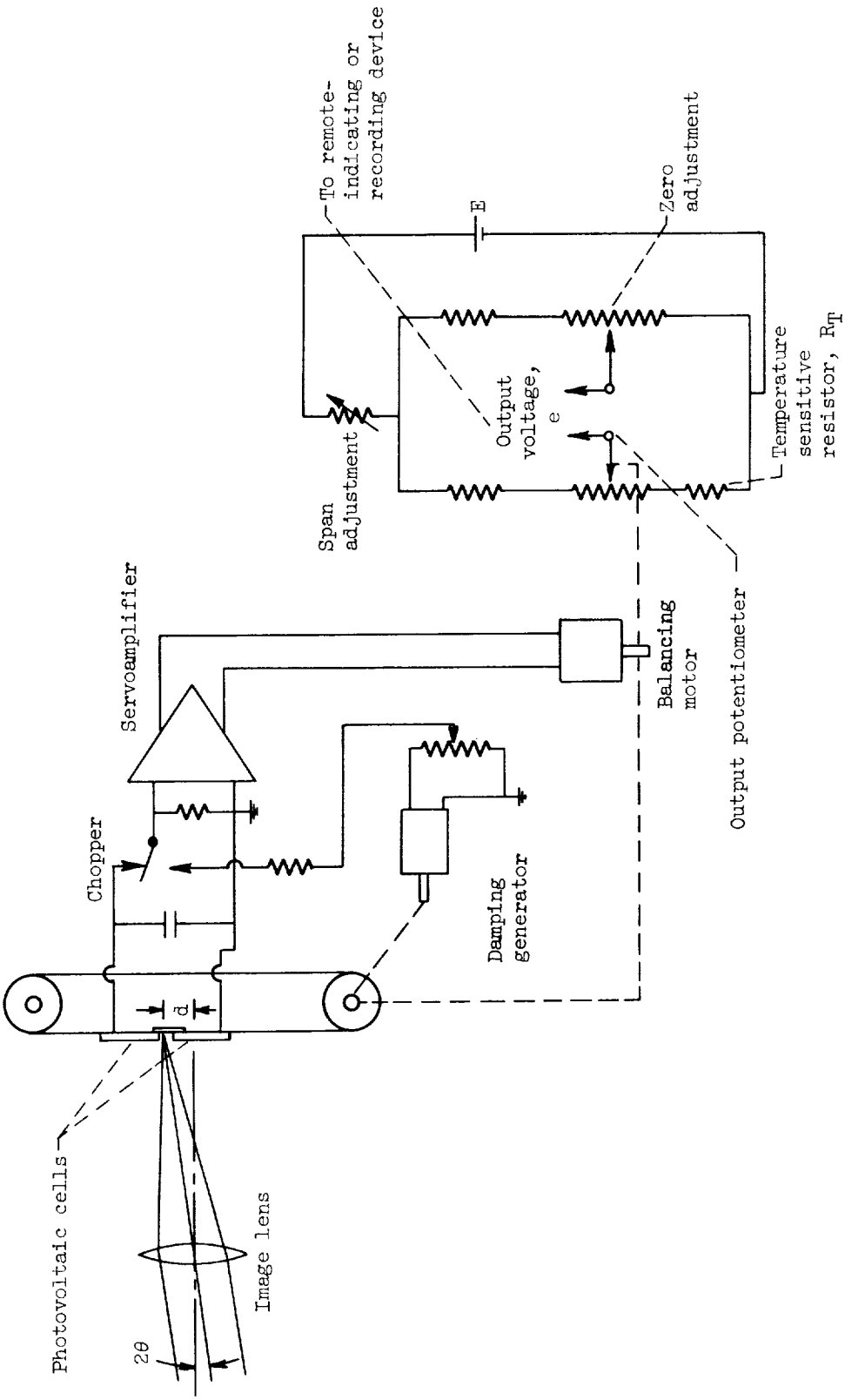

Figure 4. - Torquemeter readout servosystem.

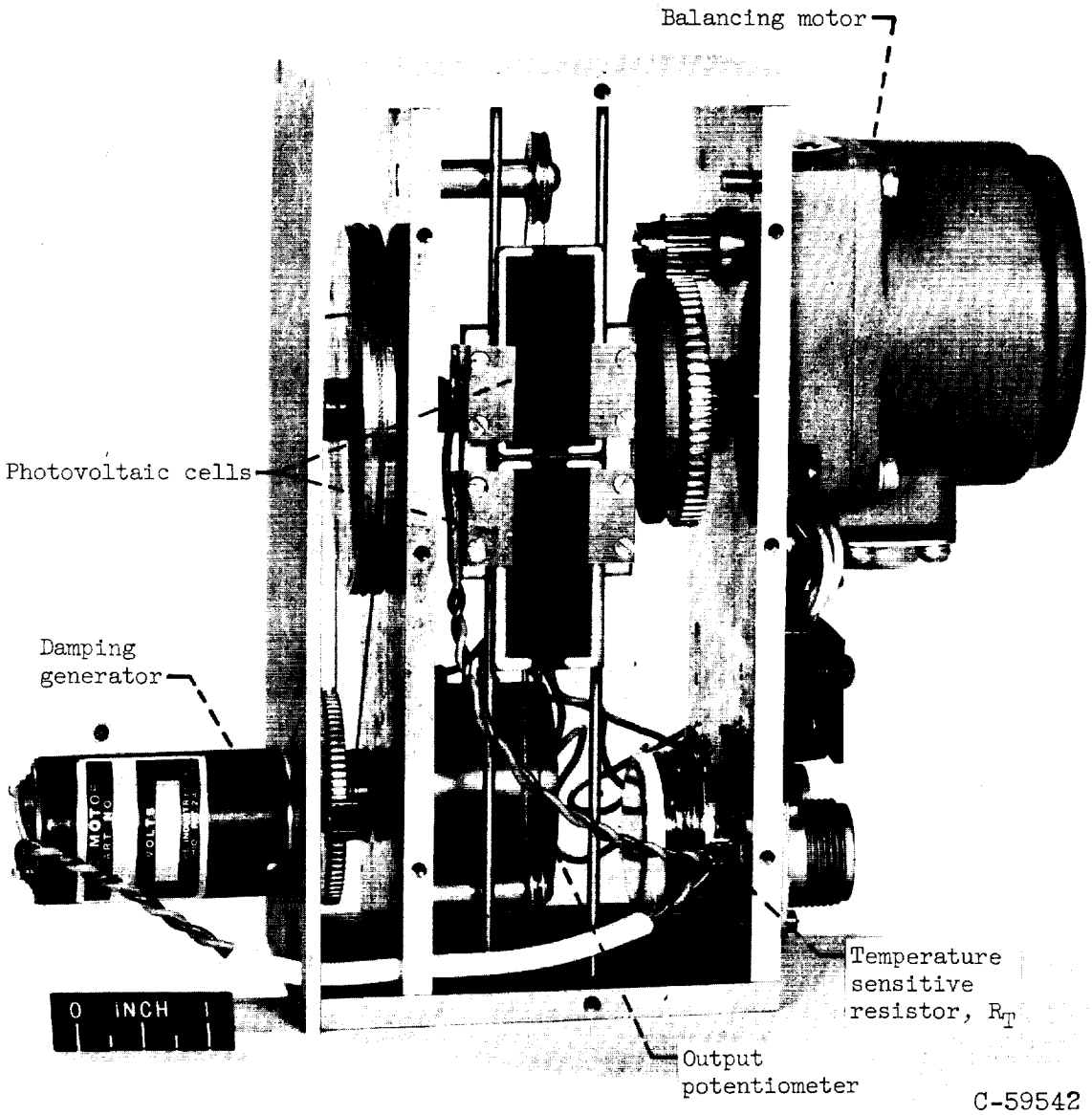

Figure 5. - Servosystem drive unit.

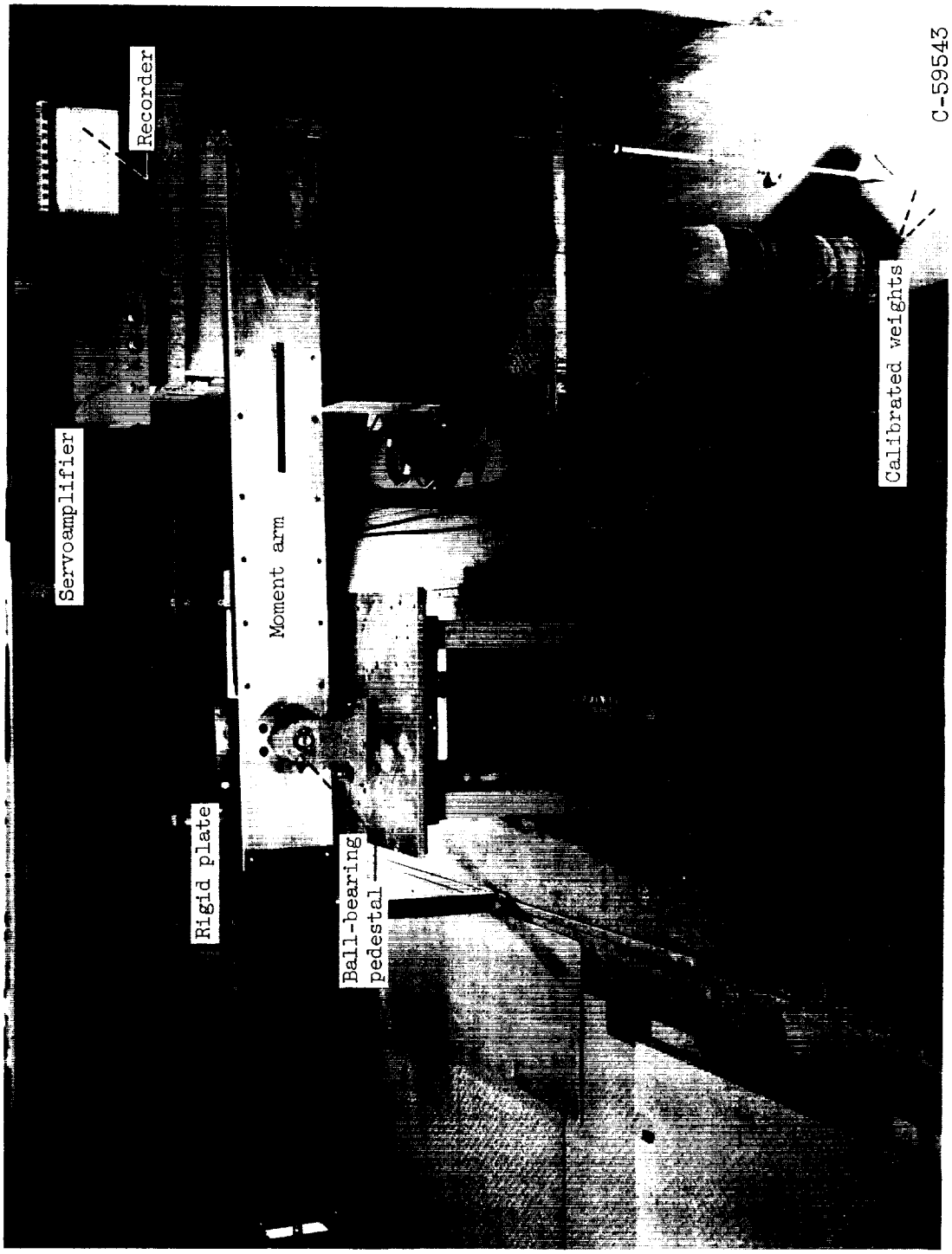

Figure 6. - Static-calibration setup.

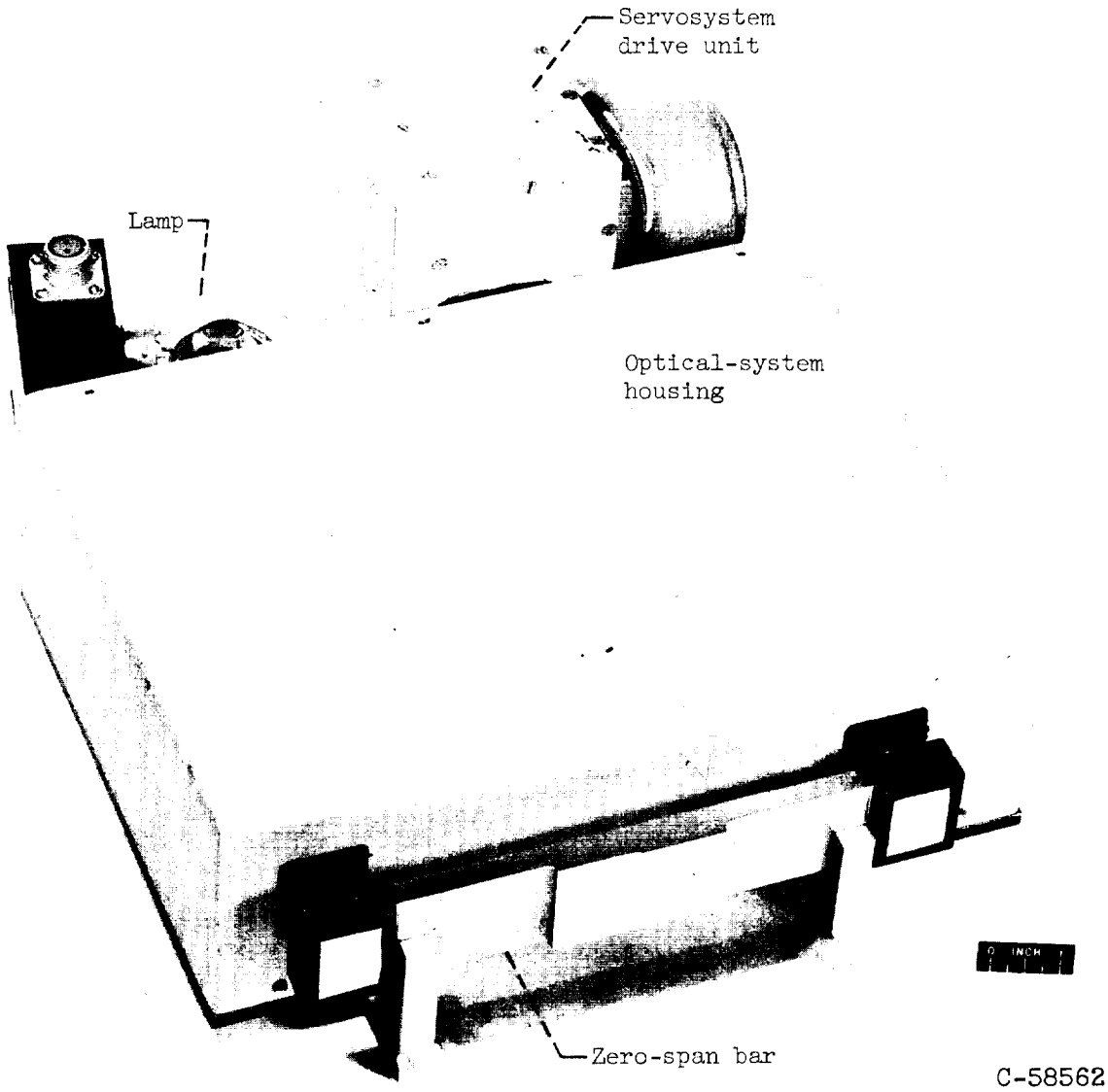

Figure 7. - Assembled torquemeter with zero-span bar in position.

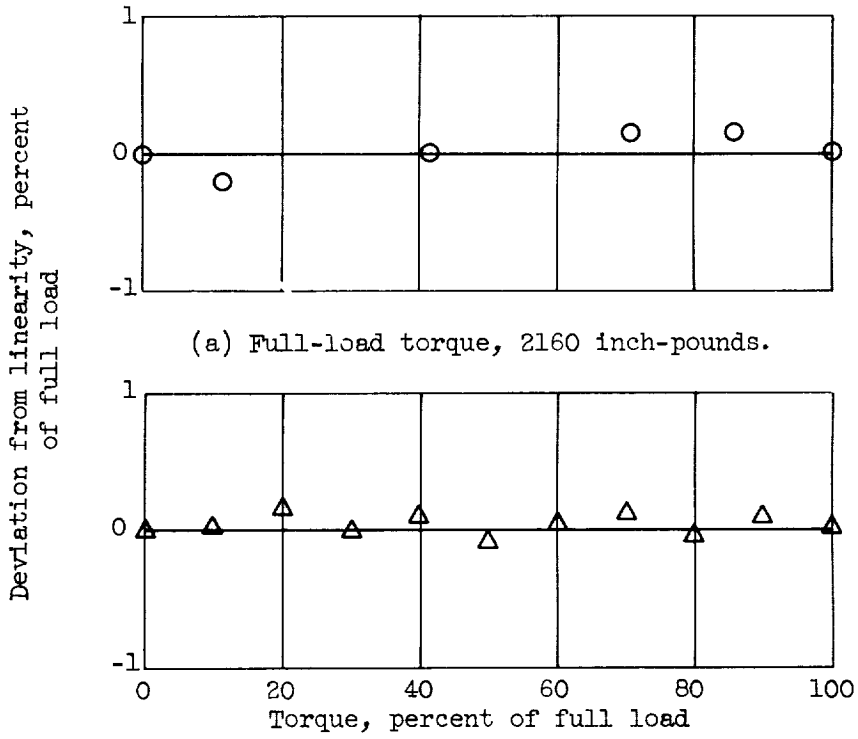

(a) Full-load torque, 2160 inch-pounds.

(b) Full-load torque, 100 inch-pounds.

Figure 8. - Static-calibration linearity.

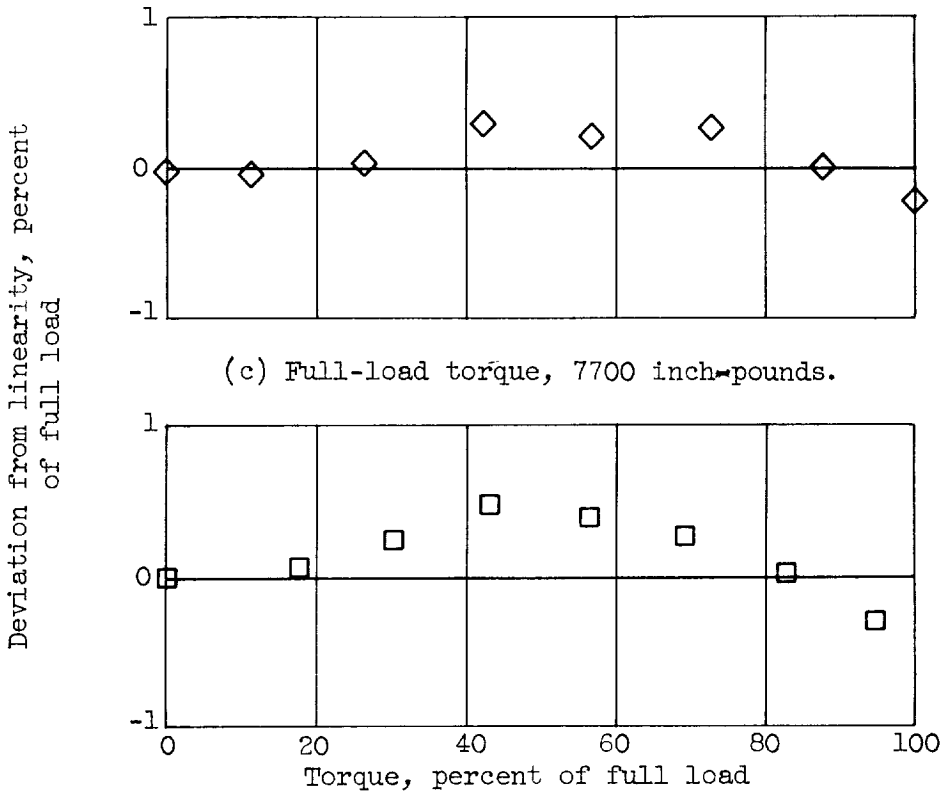

(c) Full-load torque, 7700 inch-pounds.

(d) Full-load torque, 26,400 inch-pounds.

Figure 8. - Concluded. Static-calibration linearity.

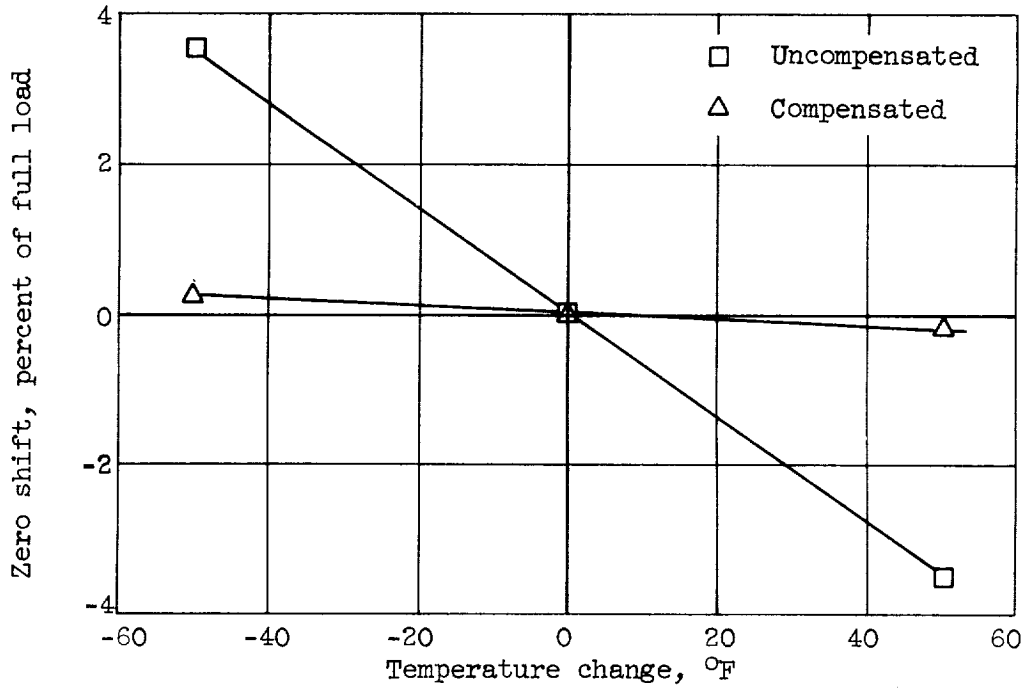

Figure 9. - Typical zero shift due to temperature change of the optical torquemeter.

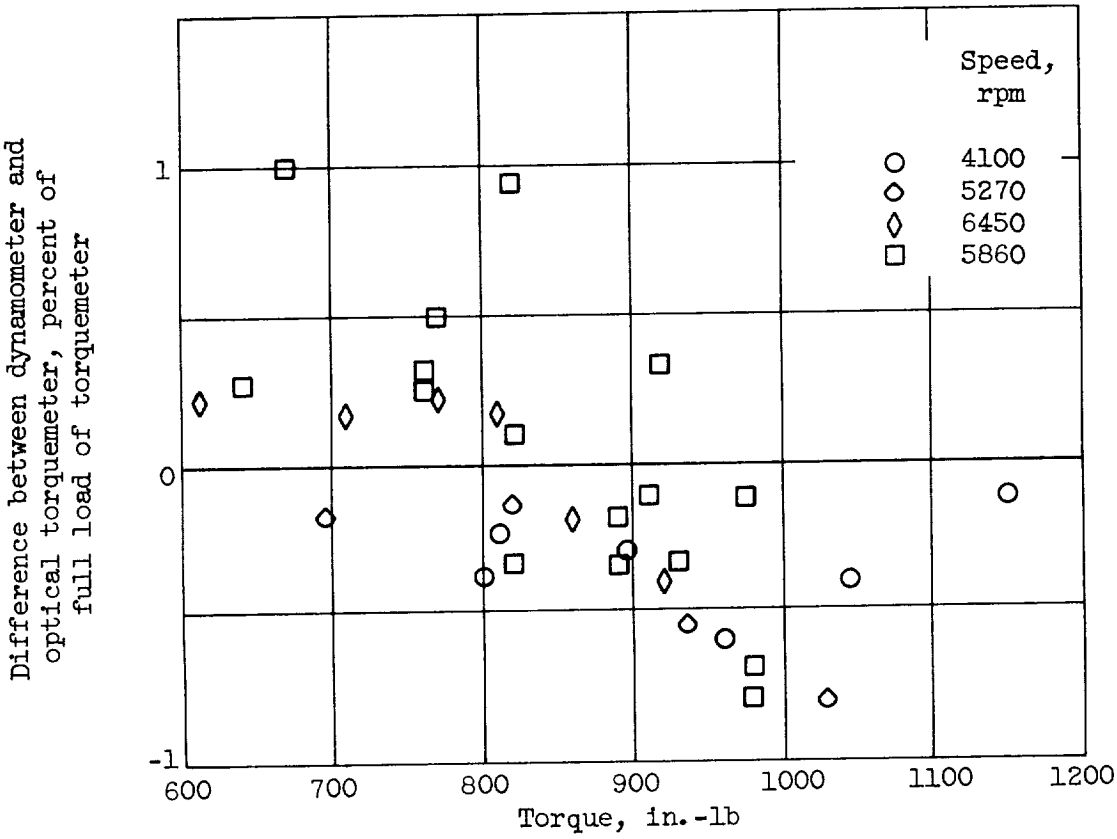

Figure 10. - Comparison of dynamometer with optical torquemeter.

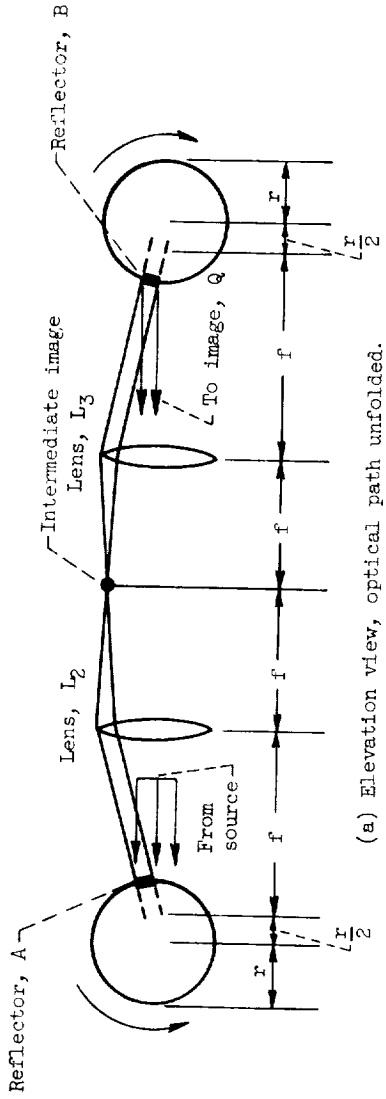

(a) Elevation view, optical path unfolded.

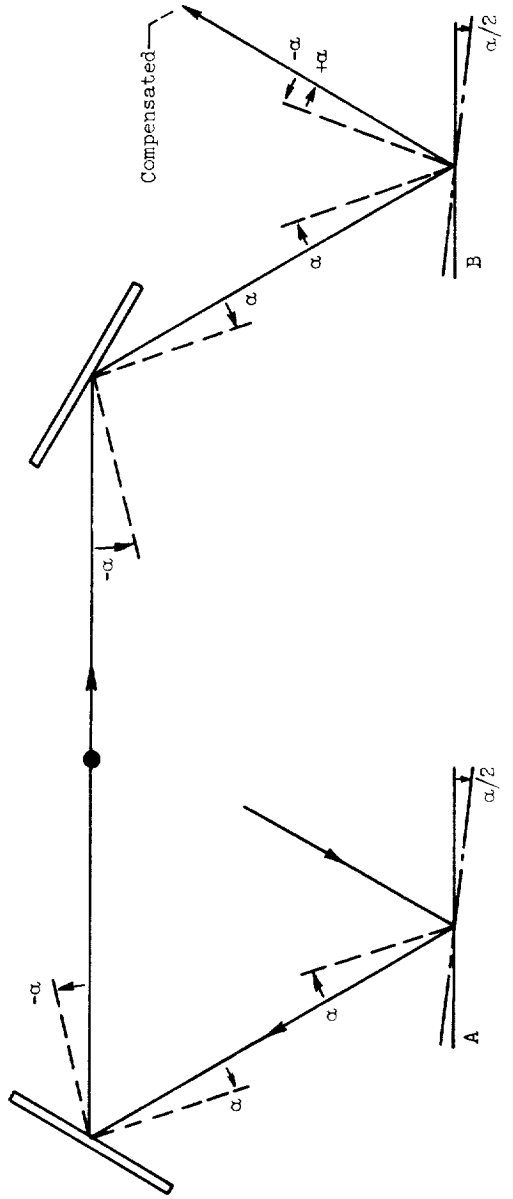

(b) Shaft rotation about vertical axis.

Figure 11. - Motion compensation.